Load-Cascading of Transient Multi-Axial Forces in Automotive Suspensions by Adams/Car

Dr. Alfons Noe

ZF Lemförder Fahrwerktechnik
Advance Development and Electronic Systems
Dielingen, Germany

1. Background and Objectives

The application of Multi Body Simulation (MBS) for the development of automotive suspension is twofold: First, MBS has become an established tool for the virtual design of full vehicle behavior. Second, the calculation as well as the assessment of internal cross sectional forces of suspension components is enabled. In this presentation, the implementation of the MBS at the ZF Lemförder Fahrwerktechnik (ZF-LFT) to achieve the required integrity for maximum strength single event load cases and fatigue load cases with respect to current suspension development is addressed.

In terms of ZF-LFT terminology the top-down process to compute forces on component or part level from given external forces and torques at wheels is named as Load-Cascading. ZF-LFT has established this process based on native Adams/Car enhanced by a special virtual Dynamic 19-Channel Suspension Testrig. It is noted that beyond classic Rigid Body MBS, it has become a frequent standard at ZF-LFT to conduct simulations with flexible Rigid Body MBS by applying Adams/Flex. This ZF-LFT-Adams-Testrig is tailored to the ZF-LFT-Hardware-Testrigs and provides various functions to treat transient, inherently highly dynamic multi-axial forces recorded from Road Load Data Collection (RLDC) but may also provided by synthetically compiled force-time series. The tracks of measured wheel center RLD forces into testing and especially Adams simulation is visualized in the figure below.

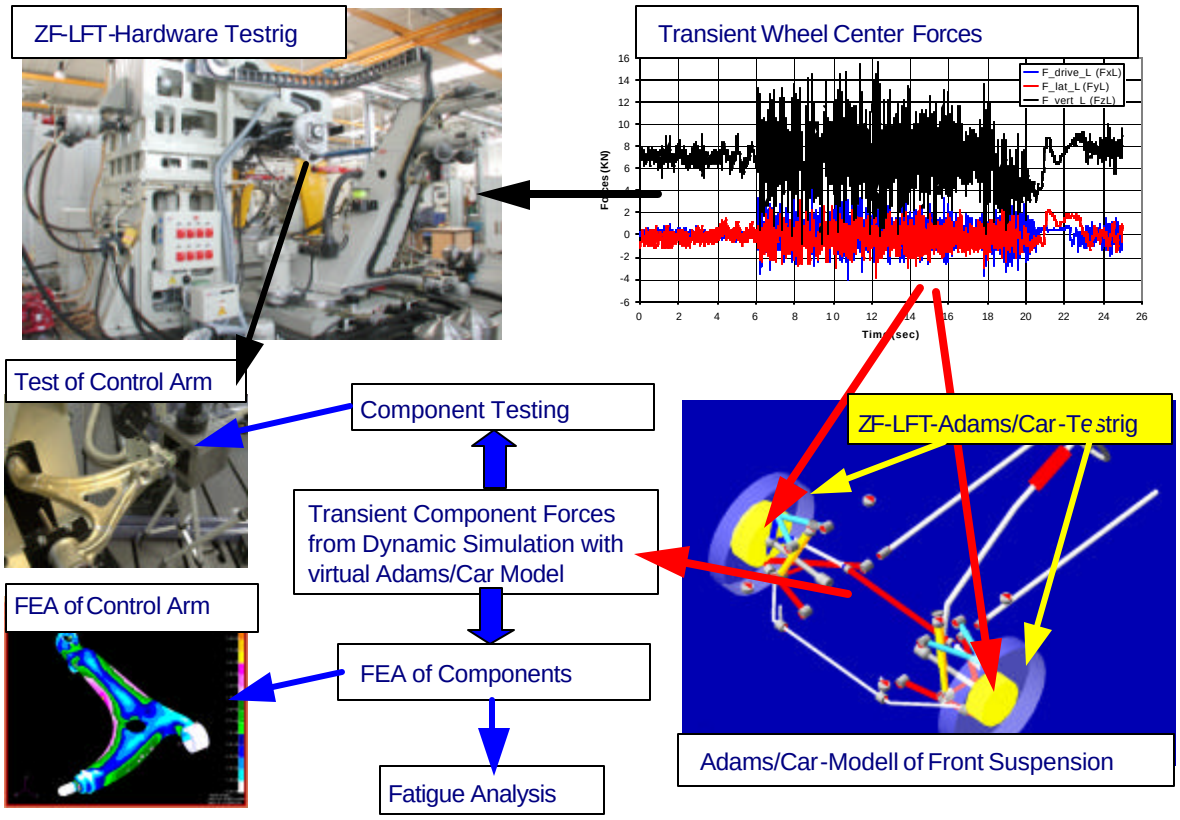

Fig. 1: Cascading of wheel center forces in a suspension for strength/fatigue calculations and testing.

2. Multi Body Dynamics for (flexible) Automotive Suspensions by Adams/Car&Flex

Along with the development process methodology in the automotive, and many other industries, ZF-LFT has established multi body simulation (MBS) by the usage of Adams/Car. Beyond classic rigid body MBS, it has become almost standard at ZF-LFT to conduct simulations with flexible rigid body MBS by applying Adams/Flex. Fig. 3 shows the multi body dynamics models of a multi link rear axle suspension in the rigid body state and the updated level with included flexible bodies for the subframe the toe links, upper links, the lower links and the wheel carriers.

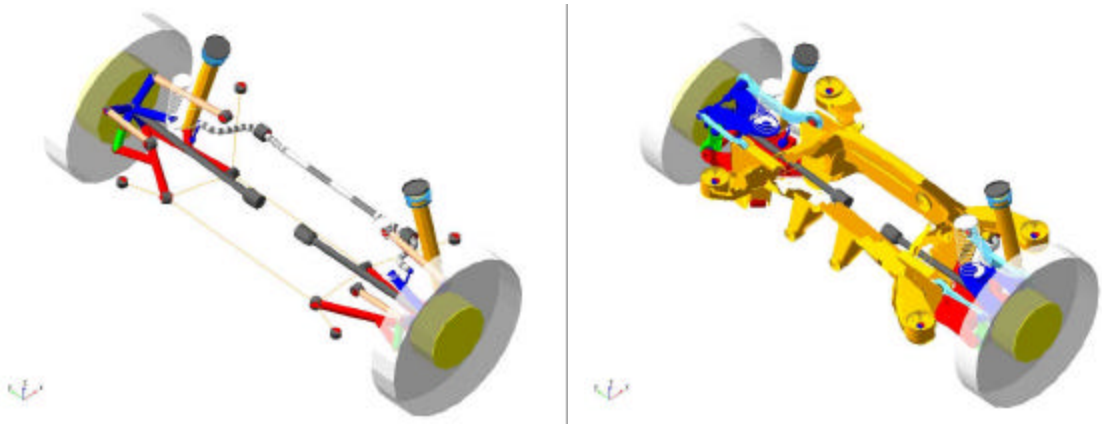

Fig. 2: Multi Link Rear Axle Suspension modeled by Adams/Car and Adams/Car&Flex.

Although the replacement of rigid by flexible parts intuitively yields more realistic mappings of suspensions and has doubtlessly provided various improved simulation results one should always consider the price of extended computational costs. Especially in the scope of load cascading large RLD times series Adams simulations of generally several 100 seconds have to be conducted. In section 4.2 of this paper the outcome of advanced flexible modeling is analyzed. Prior to this a brief review of the underlying multi body dynamics is instructive and recalls where the changes originate from.

Classical multi body dynamics formulates the equations of motions for *M* rigid bodies, which are linked together by either mass-less joints (translational, revolute, hooke) or viscose-elastic mass-less couplers (springs, dampers, bushings). The governing differential equations become non-linear, whenever large movements occur, e.g. in a typical four link suspension. The equations of motions can be derived in two forms: 1) A system of *M* with 6*M* degrees of freedom *(DOF)* is generated, which DOF are constraint by *N* algebraic constraint equations. 2) The equations of motions are expressed in minimal coordinates, which are the physical DOF (e.g. rotational angle of a joint). Although this approach is principally more sophisticated, closed chains, e.g. a double wishbone suspension, cannot be analytically eliminated and thus algebraic constraints remain. Adams has adopted the first method.

In mathematical terms, the equations of motions for a (non-conservative) multi body system consisting of rigid and flexible (elastic) parts connected by visco-elastic links and subjected to algebraic constraints can be derived from Hamiltons´s Variational Principle. The resulting set of *6M* ordinary differential equations is given by Lagrange´s equations of 2. form augmented by algebraic equations reads

$$\frac{d}{dt}\left(\frac{\partial L}{\partial \dot{?}}\right)-\frac{\partial L}{\partial ?}+\frac{\partial F}{\partial \dot{?}}+\sum_{k=1}^{N}\frac{\partial \Phi_k}{\partial ?}\,?_k=\mathbf{Q}\quad,\quad \text{Constraint}:\Phi_k(?)=\mathbf{0}\quad,\quad ?=(\mathbf{r},?,\mathbf{q}), \tag{1}$$

where *L=T-V* denotes the Lagrange Function, *T* the kinetic energy, *V* the potential energy, the non-conservative (damper) dissipation function *F*, the constraint vector Φ_k, the Lagrange multiplier for the constraints l_k and the generalized external forces **Q**. The vector of unknown **?** comprises the 6*M*-translational and rotational coordinates **r** and **?** as well as modal coordinates **q**, which represent the degrees of freedom for the flexible parts. Provided elastic deformations are geometrically small and stiffness and damping matrices **K** und **D** are constant, from equation (1) the more explicit equations of motions for a flexible multi body system in eq. (2) are obtained. Herein $\mathbf{f}_g$ is the gravitational force.

$$\mathbf{M}\ddot{\mathbf{q}} + \dot{\mathbf{M}}\dot{\mathbf{q}} - \frac{1}{2}\left(\frac{\partial \mathbf{M}}{\partial \mathbf{q}}\dot{\mathbf{q}}\right)^T \dot{\mathbf{q}} + \mathbf{K}\,\mathbf{q} + \mathbf{f}_g + \mathbf{D}\,\dot{\mathbf{q}} + \sum_{k=1}^{m} \frac{\partial \Phi_k}{\partial \mathbf{q}} \lambda_k = \mathbf{Q} \qquad , \qquad \text{Constraint} : \Phi_k(\mathbf{q}) = \mathbf{0} \quad (2)$$

It is important to realize that due to integration of part flexibility in the multi body model the mass matrix becomes non-constant. The mass matrix $\mathbf{M} = \mathbf{M}(\mathbf{q})$ depends on the unknown coordinate vector $\mathbf{q}$ and thus introduces an additional non-linearity to the multi body system, beyond non-linear kinematics and algebraic constraints. A good level of accuracy at acceptable numerical costs is attained, when modal coordinates **q** enter the mass matrix only in linear order, known as partial coupling in Adams terminology.

3. The Virtual Dynamic ZF-LFT-Adams-Testrig

The classical strength calculation (peak-loads, damage-loads) of an automotive suspension relies on a set of quasi-static load cases based upon previous experience, which also contain engineering safety factors to cover uncertainties of highly dynamic Road Load Data (RLD) characteristics. Those characteristics are misuse situations, e.g. a pothole crossing, or higher frequencies signal contents in the RLD. For example, in axle system testing, force signal information in the bandwith 50 *Hz* is evaluated, important for fatigue performance. This is approximately five times the eigen-frequency of the un-sprung masses which are around 10 *Hz*. In Adams the RLD enter the suspension via the testrig. However, the standard MDI Suspension Testrig in Adams/Car offers only the possibility for quasi-static simulations. This implies that the internal dynamics of the suspension (due to interia, dampers, springs) remains ignored and consequently applied transient wheel forces are cascaded to wrong internal forces e.g. similar to a mass-less framework. Thus, velocity-dependent damper forces are eliminated as load-carriers in the suspension. This observation and the poor capabilities of the standard MDI Suspension Testrig to process relatively large force versus time series motivated the development of the Dynamic ZF-LFT-Testrig. The standard load case file (*.lcf*-file) allows for no more than about 7000 time steps, exploiting all memory options on a HP-J6000 workstation. This time step limit restricts the evaluation of RLD sets which are approximately no more than 25 seconds long.

The access to the Dynamic ZF-LFT-Testrig is controlled by a set of command and macro files launched with the start of Adams/Car. The user input window to utilize the testrig for simulations is shown in Fig 3. The key characteristics are described in the following:

- The virtual ZF-LFT-Testrig has been tailored to the functions of the ZF-LFT Hardware Testrigs. An example is shown is in Fig. 1. The hardware testrigs offer up to 9 channels at each wheel disc, either three force and torque components at the wheel center or alternatively three force components at the wheel contact patch. The lower right part of Fig. 3 illustrates where forces and torques enter the testrig. The virtual ZF-LFT-Testrig is restricted to force/torque controlled input. This overcomes the frequent problem in Adams/Car simulations that the related specific tire model is not available although not required when measured road forces are processed. In addition to wheel loads, steering input is enabled by the virtue of the steering angle or the steering torque, respectively.
- The Dynamic ZF-LFT-Testrig has been equipped with many user input facilities to make its application most effective. Those are the individual selection of active channels, scaling and offset options as well as choosing the time interval to be analyzed and the output at step size *Dtout*. As input time series (e.g of more than 100s duration at 250 to 500 Hz) create huge requests files, but only certain requests are desired for further investigations, a reduced request file set may be selected.
- To process input time series of 10^5 up to the current upper limit of 10^6 lines, the default read-in subroutine for the *Jcf*-file and the storage of input data has been replaced by using a Fortran-subroutine by MDI. This stores splines, to be computed from the input data, much more efficiently. It is however required to install a Fortran compiler (or C++) and generate a new solver executeable out of Adams, either as a solver-private library or as a solver-site library. The ascii-type input data must be stored with the file suffix *spl* (*file-name.spl*).
- Although dynamic simulations are intended quasi-static simulations remain available. By default the time integration is performed by integrator type GStiff, in which the constraint vector Φ_k is evaluated at

position level (Index 3). Alternatively the usually more accurate and robust but slower index 2 stabilized solver SI2 is offered. The SI2 solver evaluates constraint at velocity level, that is the time derivatives of the constraint vector. Simulations are often carried out using the same Adams model but with minor changes to input forces files or e.g. non optimized integration errors. This requires changes only to the simulation control file **.acf*, the default mode of simulation can be changed from *Interactive* to *Batch* which only generates the files **.acf*, *.adm and **.nam*. The solver run itself is then operated in a Unix shell or in a DOS window. The batch mode provides the additional benefit that the Adams/Car license is free for continuing the modeling process.

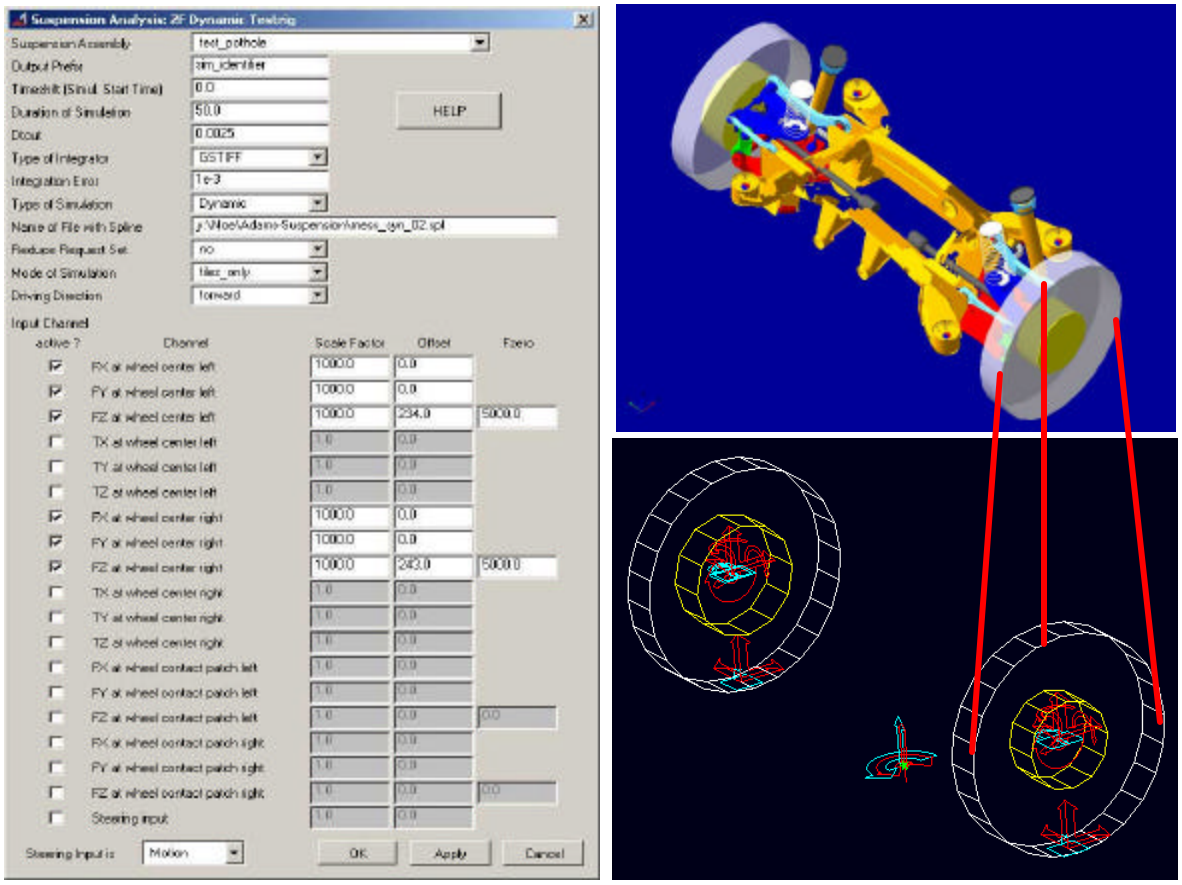

Fig. 3: Functions of the Virtual Dynamic ZF-LFT Suspension Testrig (ZF-LFT-Adams-Testrig).

4. Application of the Virtual Dynamic ZF-LFT-ADAMS-Testrig to Synthetic RLD

Before the Dynamic ZF-LFT-Testrig is utilized for the load cascading of measured Road Load Data Collections (RLDC), it is first applied to synthetic wheel center forces (or synthetic Road Load Data). This strategy not only provides familiarity with the testrig performance but, firstly, generates quantitative insights as to how dynamic excitation at the wheels is dynamically transferred to internal attachments points, in comparison to quasi-static transfer. This objective is studied via the use of harmonic (sinusoidal) wheel center forces. Secondly, the benefits of flexible versus rigid modeling are investigated by simulating a pothole crossing. Thirdly, the influence of the selected numerical solver and error tolerances upon the required accuracy of internal force determination is briefly addressed. The analysis has been carried out for two different multi link rear axles similar to the axle in figure 2.

4.1 Harmonic Wheel Center Loads

The harmonic (sinusoidal) wheel center force components are depicted in figure 4. They are simultaneously applied to both wheel centers. The vertical force F_z oscillates around its static mean force

F_{z0} = 7000 N at an amplitude of 3000 N, which reflects realistic scenarios in a RLDC. Artificial harmonic in-phase forces F_x and F_y in reverse longitudinal and lateral direction have been added. The force functions are built from blocks with constant frequency each, starting at 0.5 *Hz* and ending at 60 *Hz*. The related FFT-spectrum shows the sequence of frequencies. The chosen sampling frequency 370 *Hz* has been adopted from measurement conditions.

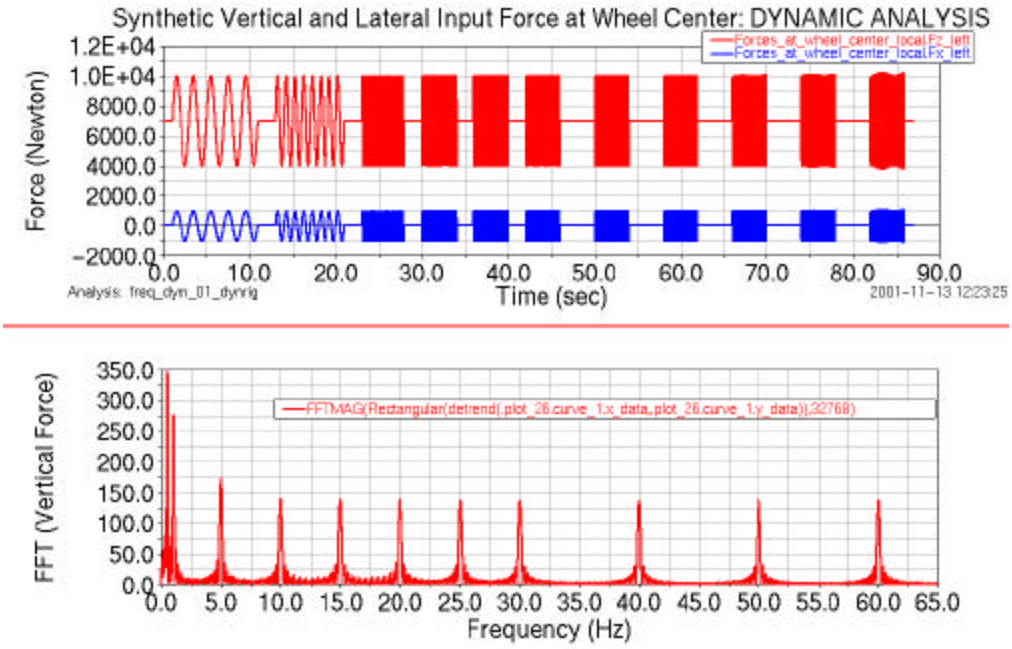

Fig. 4: Harmonic wheel center forces.

In Fig. 5, the spring and damper forces according to Fig. 4 are compared for both quasi-static and the dynamic simulation, as obtained from the standard MDI-Suspension-Testrig and Dynamic ZF-LFT Testrig, respectively. The calculation error of the quasi-static simulation is apparent, because the damper force is shown as being zero. The *real* dynamic simulation computes a relative velocity between the piston and rod which consequently provides the velocity dependent damper force. The damper force amplitude varies with the applied frequency sweep and reaches its maximum at about 10 *Hz*. This force maximum is in the region of the eigen-frequency for the wheel (being between 12 13 *Hz*) and is usually a relevant peak load to be chosen for strength calculation in finite element analysis. Recall that the amplitude versus applied frequency transfer function is well known from the basic mechanics Spring-Mass-Damper-System excited by a sinusoidal forces. Note also that the damper amplitude reaches the level of the frequency dependent spring force amplitude. The dynamic as well as the quasi-static spring force consists of a constant part (due to the static wheel center force 7 KN) superimposed with an oscillating force part. The quasi-static spring force shows the same amplitude range along the whole frequency sweep, because inertia and viscose damper forces are ignored; this error increases with the increase in frequency. As in this specific axle, the spring and damper are located at geometrically distant points on the lower control arm. Due to the non-existent damper forces, there are significant errors in the force magnitude and distribution upon the control arm. These subsequent errors, if not recognized, will introduce errors into the control arm design process, and consequently will lead to a component that fails unexpectedly early during testing. Also note that at 5 *Hz* the maximum dynamic spring force is higher than the maximum quasi-static spring force.

Figure 6 illustrates the response of the bushing, which connects the rear knuckle (wheel carrier) to the rear upper control arm, when caused by the harmonic load in Fig. 4. The impact of the force amplitudes is different for each for component and for the bushing force magnitude, e.g. the maximum values arise at mutually different applied frequencies. This force transfer behavior is partly a consequence of anisotropic bushing stiffness properties. It is also a result of the spatially varying suspension stiffness. The quasi-static simulation would have provided constant amplitudes with respect to the frequency sweep.

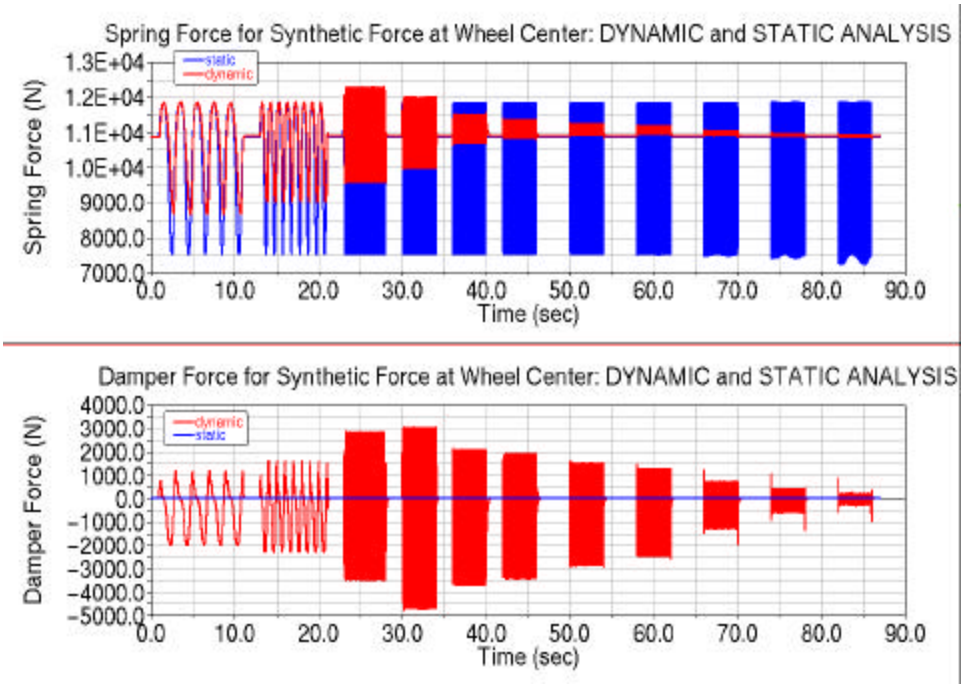

Fig. 5: Spring and damper forces for dynamic and static simulation from harmonic wheel center forces.

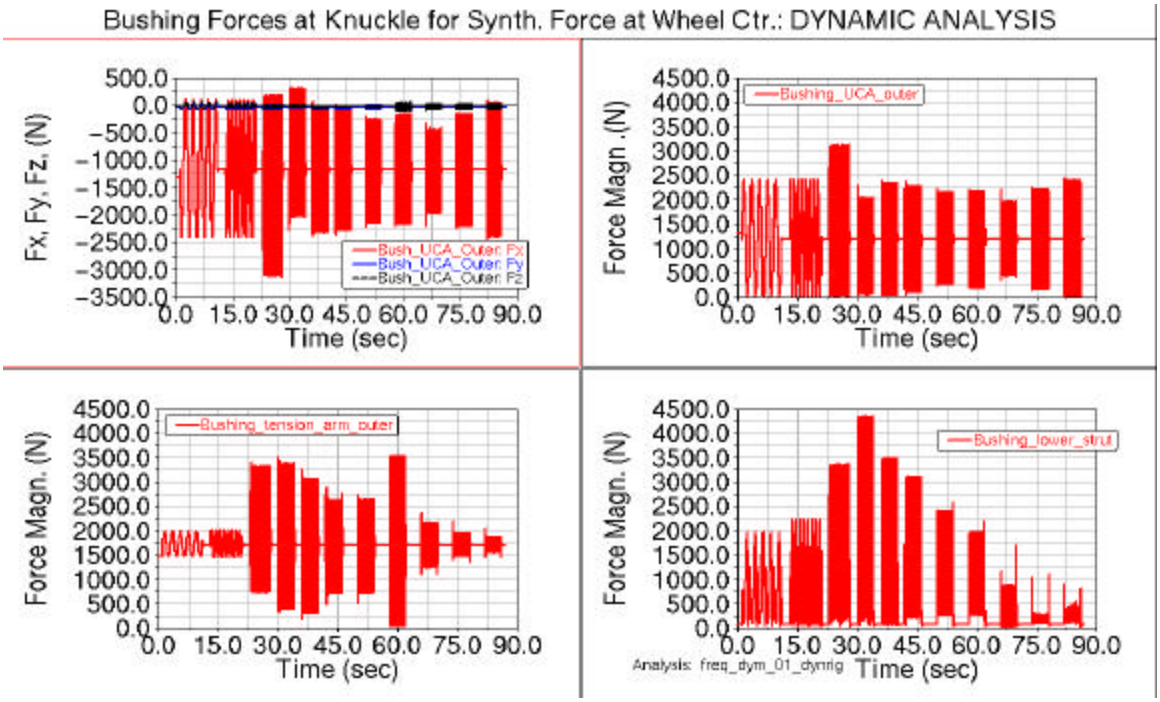

Fig. 6: Frequency dependence of bushing force amplitudes.

4.2 Pothole Crossing

In this section, the response of a multi link rear axle suspension due to a pothole crossing is investigated. This misuse-maneuver is characterized by an extremely dynamic impact situation and its accurate simulation is of great practical interest. In addition to the previous analysis of comparing dynamic vs. quasi-static simulation, the influence of generating multi-body suspension models by the means of Adams/Flex is addressed. Furthermore, the differences in using the SI2-solver (index 2) compared to the standard GStiff-solver (index 3) are outlined, along with the consideration of numerical error control.

The force components of the wheel center have been approximated by an analytical function of the type: $F(t) = F_0 \, (t/T)^{\,n} e^{-m\,(t/T)} \sin kt$. The force is scaled by a time constant *T*, which covers the typical duration of a pothole crossing event (usually of the order 10 ms). For simulation studies it is assumed that both wheels cross the pothole profile at the same time. For simplicity, the lateral y-components of the wheel center forces have been ignored. The force formulas have been sampled at 400 *Hz* or 2.5 *ms*.

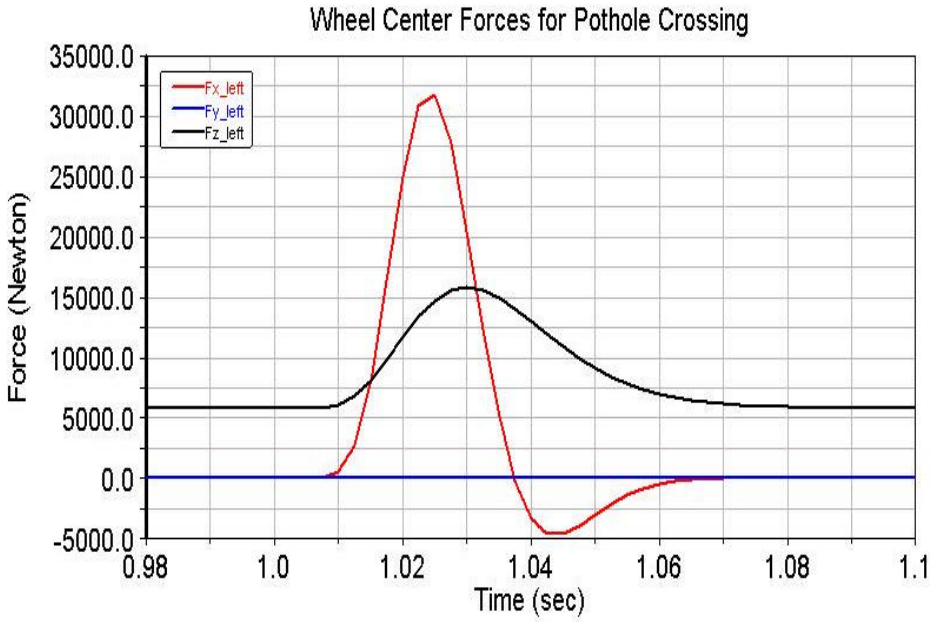

Fig. 7: Wheel center forces for pothole crossing.

By comparing the simulation option: dynamic versus quasi-static, and the modeling option: rigid versus flexible, in Adams/Car, the following graphs clearly indicate that it is more accurate to conduct a dynamic simulation. In this respect, introducing flexible parts is a second order model upgrade. However, it must be kept in mind that in terms of fatigue strength calculation a 10 percent force error introduces a lifetime error of 30 to 50 percent. Furthermore, in the scope of weight reduction, errors in peak load calculation will lead to a failed weight target.

Figure 8 shows the compressive force in the upper link. It is seen that the static simulation underestimates the maximum link force magnitude by about 4 KN. This result points out that in specific components dynamically calculated forces are not always smaller than those calculated statically. At first sight, one would expect that the material constituents (inertial and damping properties) would make the suspension more compliant and thus reduce the force level. By also referring to the spring and damper forces in Fig. 5, the maximum dynamic spring force is higher than the maximum quasi-static spring force. Furthermore, the flexible model results in figure 8 yield changes in force magnitudes of 0.3 KN, which is less than 10 percent.

An overall picture of the link force distribution in the case of the flexible multi axle link suspension is given in Fig. 9. The solid lines depict the dynamically calculated forces in the lower link, toe link, upper link and the longitudinal link, whereas the dashed lines show the static forces. As a reference the longitudinal component of the wheel center force has been added. At this scale the dynamic forces exceed the static forces by less than 20 percent. A careful analysis reveals that the dynamics can re-distribute force levels and functional shape in the arrangement of longitudinal and lateral suspension links. The zigzags in the lower and longitudinal link curves indicate that a link may have been excited (inducing oscillations or buckling) during the actual pothole impact. Such a maximum overshot represents the maximum force during that pothole crossing and is important to know for the FEA misuse calculations. This extreme force value would have been overlooked in a quasi-static simulation. The zigzags, in themselves, result from insufficient resolution of the output data step size, which is 2.5 *ms (or 400Hz)*.

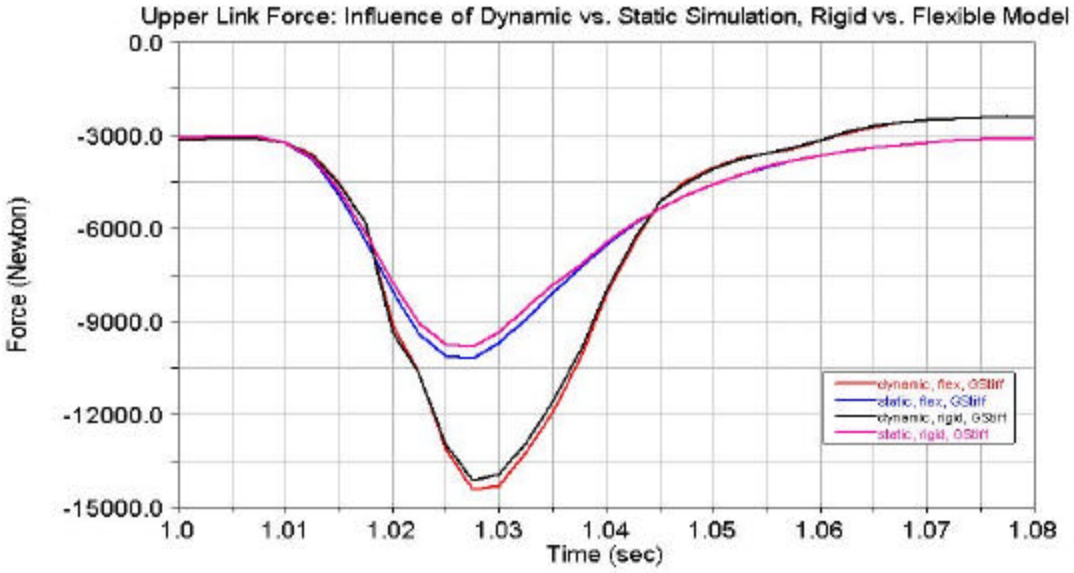

Fig. 8: Influence of dynamic vs. static simulation and rigid vs. flexible Adams model on upper link force.

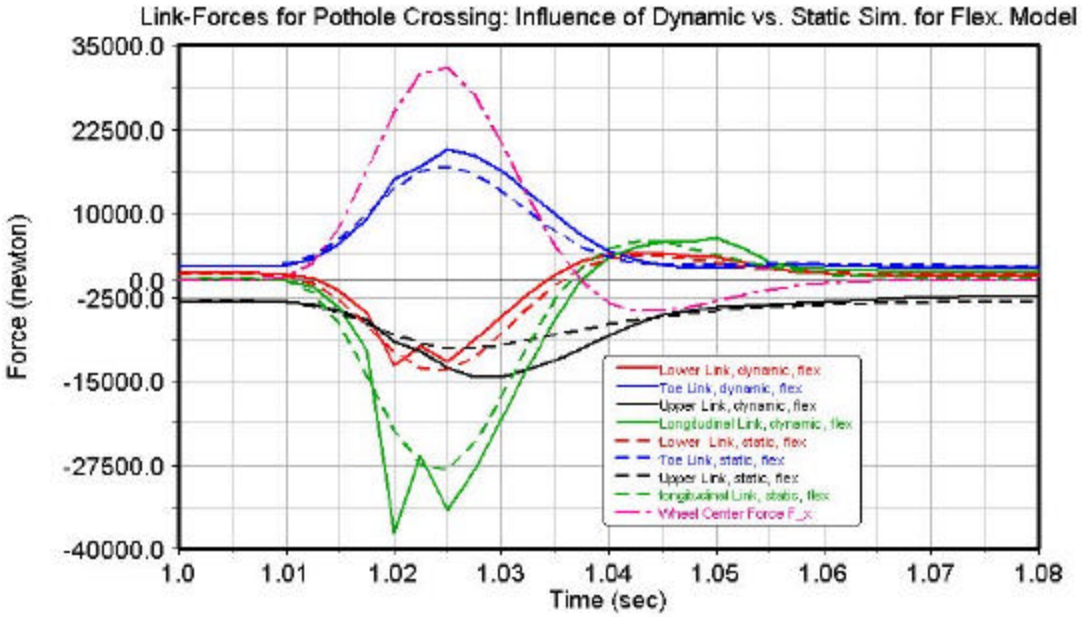

Fig. 9: Influence of dynamic vs. static simulation link forces (lower link, toe link, upper link, longitudinal link) in the case of a flexible Adams model.

Because force controlled simulations are conducted by this testrig, the influence of body inertia and the *visibility* of time decay constants due to viscous dampers can be demonstrated best by virtue of the vertical wheel travel analysis. Figure 10 shows the wheel travel for the cases dynamic vs. quasi- static simulation. To visualize, the time scale of the pothole crossing the vertical wheel center force component has been added. Similar to previous graphs the model flexibility causes second order changes. However the basic understanding is confirmed that using compliant (flexible) suspension parts increase any deflection for a given force. In summary, wheel travel is increased during the quasi-static simulation, due to the absence of inertial forces on the wheel mass (unsprung mass). Compared to the quasi-static wheel center travel, which, in duration, is the same as the pothole force, the dynamic wheel travel decays several times slower. This behavior directly reflects the damper viscosity. In the quasi-static case any damper is inactive.

In the scope of numerical integration, body inertia can be regarded as a damper. The numerically difficult start of the integration process becomes easier when sudden changes of input forces are damped out or by-passed to give numerically desirable (i.e. smooth) functions to integrate. Figure 10 shows a dip in the wheel center force at the beginning of the pothole. For the dynamic simulation case the wheel travel does not recognize the force discontinuity.

In the case of quasi-static, force controlled motions of compliant parts, e.g. a spring or bumpstop, generate not only artificially elevated displacements but also artificially increased forces, as with spring and bumpstop forces. When those forces are used for component testing early failure is likely to occur, which may trigger a new design loop based on non-existing forces. This conclusion also holds for Fig. 11, which shows the longitudinal x-displacement in the subframe-to-body-bushing. Even for a linear bushing the longitudinal bushing force is too large by 50 percent.

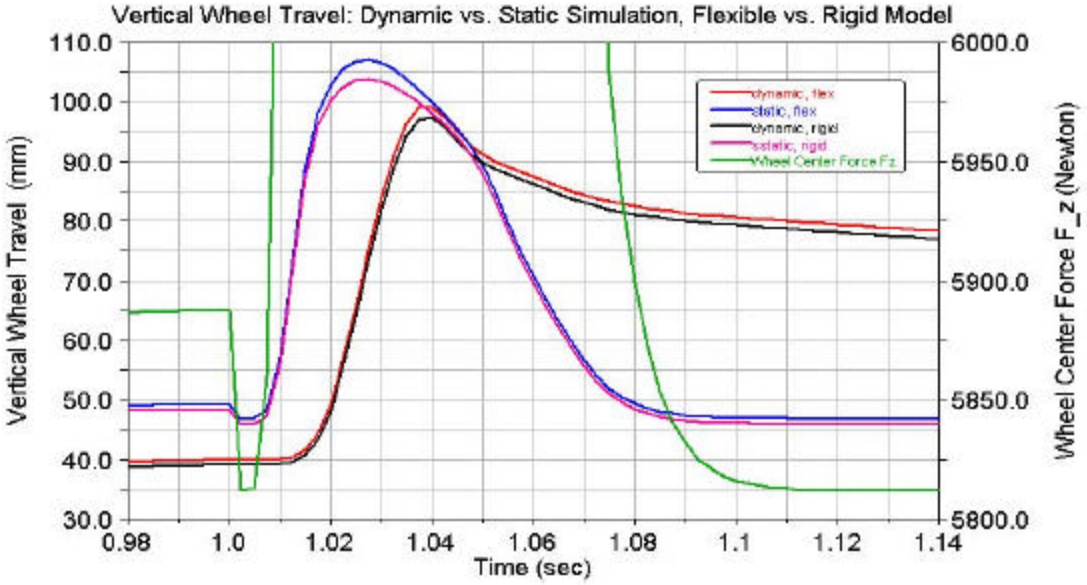

Fig. 10: Influence of dynamic vs. static simulation and rigid vs. flexible Adams model on vertical wheel center travel

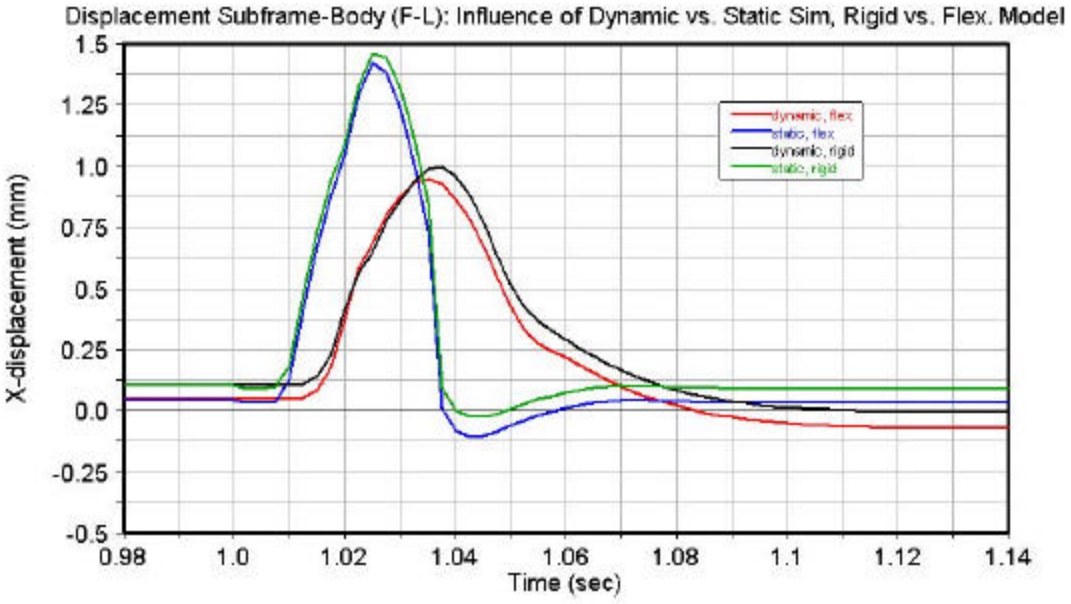

Fig. 11: Influence of dynamic vs. static simulation and rigid vs. flexible Adams model on displacements at the interface: body to subframe (bushing at front left side, displ. in longitudinal x-direction).

4.3 Selection of Numerical Solver and Integration Error

To judge which numerical solver and integration error to select with respect to the precision demands of load cascading (force/torque) at reasonable numerical costs, the results obtained from the index-3 solver GStiff are compared to those of the, as proposed, more robust and accurate but slower, index-2 solver SI2. Moreover, the integration errors 10^{-2} and 10^{-3} are analyzed. Maximum displacement errors are addressed in Fig. 12. The details show that the GStiff solver determines the same results for both error tolerances. The maximum relative output difference to the SI2 solver is 2/3 of a percent. The GStiff results are more precise, because the index-3 formulation yields the smallest errors on displacement level, whereas minimum velocity errors arise in the index-2 case. Force errors are focussed upon in Fig.13. It is seen that the integration error affects the force results. The GStiff error tolerance 10^{-2} corresponds to the force deviation of 3.5 percent compared to GStiff with 10^{-3} error tolerance. This difference enters the scope of practical relevance. The deviation between GStiff with 10^{-3} and SI2 with 10^{-3} reaches 1.4 percent. More comparisons of the last pair have been made. Differences of more than one percent are rare. In conclusion, the extra time costs for numerical integration with the SI2 are not justified.

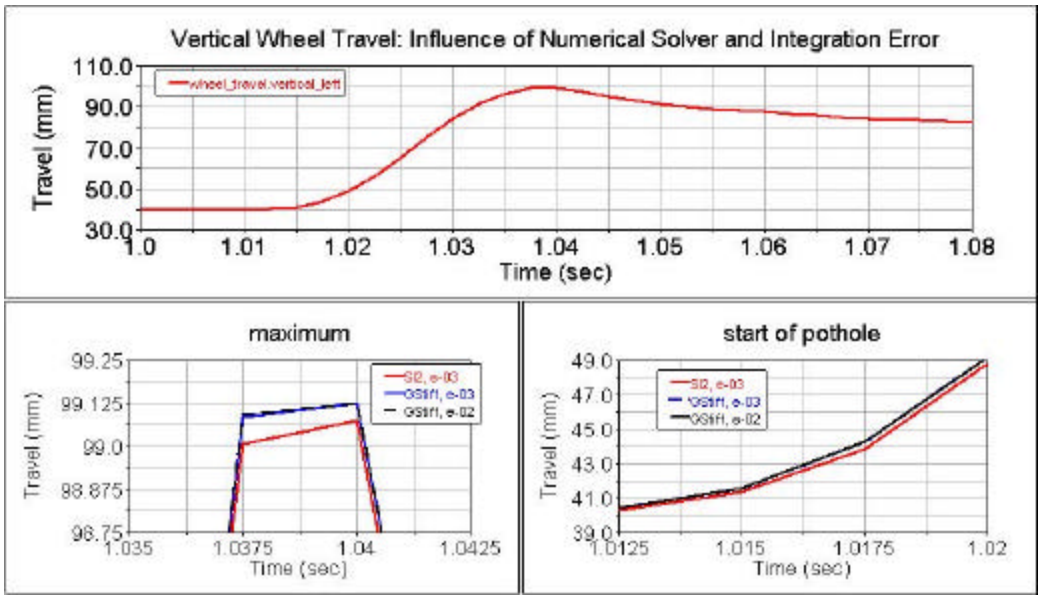

Fig. 12: Influence of numerical solver (GStiff, SI2) and integration error on vertical wheel travel.

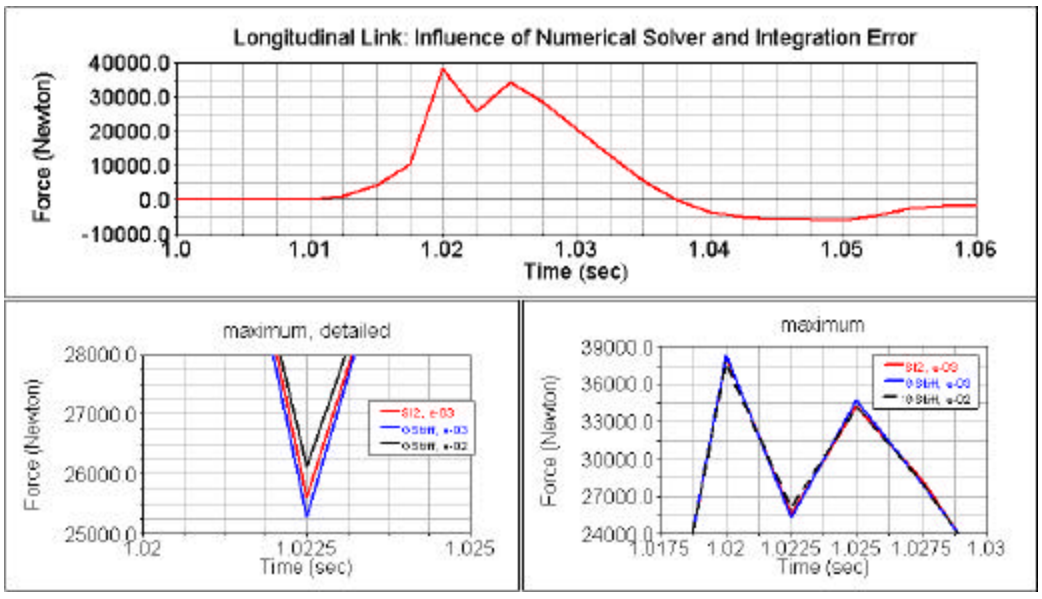

Fig. 13: Influence of numerical solver (GStiff, SI2) and integration error on force in longitudinal link.